7th ECCOMAS Thematic Conference on Smart Structures and Materials
SMART 2015
A.L. Araúo, C.A. Mota Soares, et al. (Editors)

MECHANICAL DEGRADATION AND LIFETIME PREDICTION OF TETRAGONAL FERROELECTRICS UNDER CYCLIC ELECTROMECHANICAL LOADING

Stephan Lange[*], **Andreas Ricoeur**[†]

[*,†]University of Kassel, Institute of Mechanics, Chair of Engineering Mechanics / Continuum Mechanics
Mönchebergstr. 7, 34125 Kassel, Germany

[*]stephan.lange@uni-kassel.de
[†]ricoeur@uni-kassel.de

Keywords: Ferroelectrics, tetragonal unit cells, grain interaction, residual stresses, high cycle fatigue, lifetime prediction.

Summary: *Reliability and life time of smart materials are crucial features for the development and design of actuator and sensor devices. Being widely used and exhibiting brittle failure characteristics, ceramic ferroelectrics are of particular interest in this field. Due to manifold interactions of the complex nonlinear constitutive behavior on the one hand and the damage evolution in terms of microcrack growth on the other, modeling and simulation are inevitable to investigate influence parameters on strength, reliability and life time. The so-called condensed approach, which is presented first, considers just one characteristic point in the material, nonetheless accounting for polycrystalline grain interactions. Then, a model to predict the lifetime in terms of high cycle fatigue under electromechanical loading conditions is introduced.*

1. INTRODUCTION

Ferroelectric materials such as barium titanate (BT) or lead zirconate titanate (PZT) have been established as components of so-called smart structures during the past few decades. They are used as bulk material in actuators or sensors and are constitutents of micro electromechanical systems (MEMS) and composite devices. To model the nonlinear behavior of ferroelectric materials, a variety of models has been published during the past decades. HWANG et al. [1] propose a model that assumes a polycrystal with monodomain grains, where the polarization switches by a discrete angle if an energetic switching criterion is satisfied. In HUBER et al. [2], scalar weights are introduced for each orientation of the c-axis of a tetragonal unit cell within a grain. Within the context of material theory, they have to be interpreted as internal variables controlling all dissipative processes. Their evolution is governed by energetic considerations based on the first and second principles of thermodynamics. Most of the approaches that have been developed are implemented within the framework of the Finite Element Method (FEM),

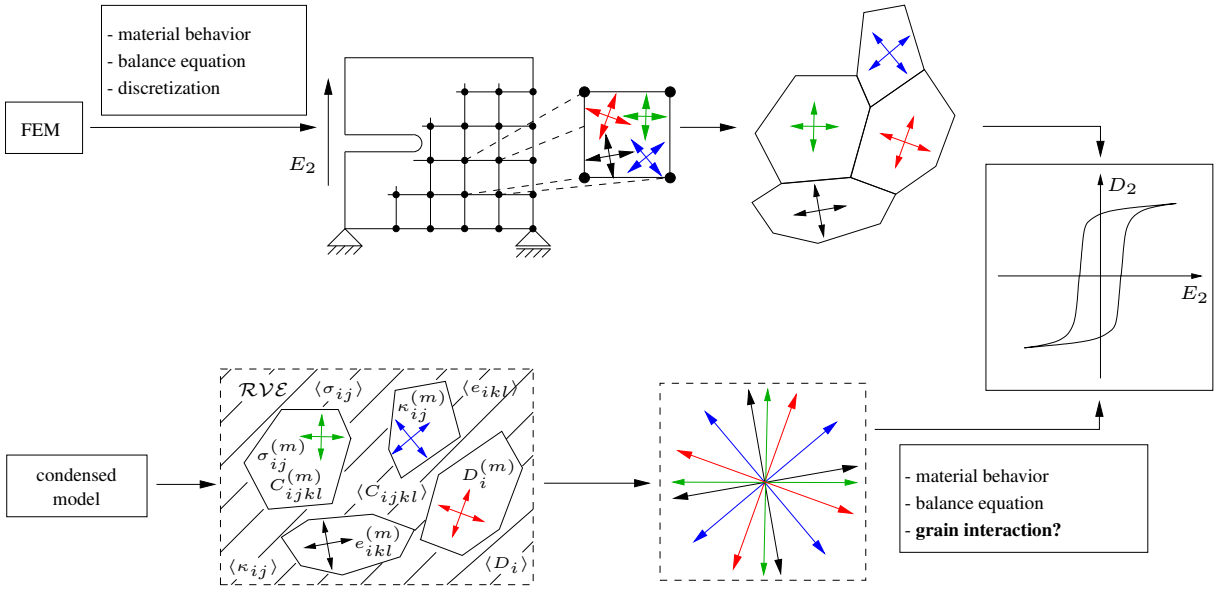

Figure 1. Illustration of the principles of FE and condensed approaches

enabling the solution of complex boundary value problems (see Fig. 1). On the other hand, the implementation of a discretization scheme is going along with a high effort and the solution of problems requires high computational costs. However, many results shown in papers are restricted to very basic boundary value problems under uniaxial loading. The goal mostly is to calculate different hysteresis loops of tetragonal ferroelectrics, thus demonstrating and investigating their constitutive behavior. This kind of investigation, however, does not require the application of a discretization method.

Following the introduced model by LANGE AND RICOEUR [3], the grains are embedded into an effective medium and condensed to a single material point (see Fig. 1). The interaction between grains is taken into account applying an averaging technique calculating effective inelastic mechanical and electrical fields for a polycrystalline material. The computational and implementation effort going along with the condensed model is low compared to FEM based approaches. Nevertheless, all essential features are included yielding smooth hysteresis loops of the bulk material under combined electromechnical load and residual stresses in each grain. To predict the lifetime of ferroelectric materials under cyclic electromechanical loading, a model for high cycle fatigue is presented based on the condensed model.

2. A CONDENSED MODEL FOR POLYCRYSTALLINE FERROELECTRICS

Neglecting volume forces and charges, the balance equations of mechanical and electrostatic equilibrium are reduced to:

$$\begin{aligned} \sigma_{ij,j} &= 0, \\ D_{i,i} &= 0, \end{aligned} \tag{1}$$

where $(\ldots)_{,j} = \partial/\partial_j$ describes the partial differentiation with respect to x_j. σ_{ij} and D_i are the associated variables stress and electric displacement. Starting from the first law of thermodynamics, considering Eq. (1), static limits $\dot{u}_i = \ddot{u}_i = 0$, the divergence theorem, the Cauchy theorem $t_i = \sigma_{ij}\, n_i$ and $\dot{\omega}_S = -\dot{D}_i\, n_i$ as well as the relations $E_i = -\varphi_{,i}$ and $\sigma_{ij}\, \dot{u}_{i,j} = \sigma_{ij}\, \dot{\varepsilon}_{ij}$, the local formulation of the energy balance is finally obtained as [3]:

$$\dot{u} = \sigma_{ij}\, \left(\dot{\varepsilon}_{ij}^{\mathrm{rev}} + \dot{\varepsilon}_{ij}^{\mathrm{irr}}\right) + E_i\, \left(\dot{D}_i^{\mathrm{rev}} + \dot{P}_i^{\mathrm{irr}}\right) - q_{i,i} + \rho\, r. \tag{2}$$

The terms $\dot{\varepsilon}_{ij}^{\mathrm{irr}}$ and $\dot{P}_i^{\mathrm{irr}}$ describe the irreversible strain and polarization rates as results of domain wall motion. Thermodynamic consistency requires the satisfaction of the second law of thermodynamics (e.g. [4])

$$\theta\, \dot{s} + q_{i,i} - \frac{q_i}{\theta}\, \frac{\partial \theta}{\partial x_i} - \rho\, r \geq 0 \tag{3}$$

where s is the specific entropy. Inserting Eq. (2) into Eq. (3) yields in the generalized CLAUSIUS-DUHEM-inequality. PATRON AND KUDRYAVTSEV [4] discussed the generalized inequality for $\dot{\varepsilon}_{ij}^{\mathrm{irr}} = 0$ and $\dot{P}_i^{\mathrm{irr}} = 0$ and showed that it holds for any values of $\dot{\varepsilon}_{ij}^{\mathrm{rev}}$, $\dot{D}_i^{\mathrm{rev}}$ and $\dot{s}$ leaving the statement $q_i\, \theta_{,i}/\theta \geq 0$. Thus, considering domain switching as further irreversible processes, the inequality reads

$$\sigma_{ij}\, \dot{\varepsilon}_{ij}^{\mathrm{irr}} + E_i\, \dot{P}_i^{\mathrm{irr}} - \frac{q_i}{\theta}\, \frac{\partial \theta}{\partial x_i} \geq 0. \tag{4}$$

Eq. (4) is of essential significance for the development of a thermodynamically consistent microstructural evolution law.

The nonlinear thermodynamic potential of a ferroelectric material is introduced as:

$$\begin{aligned} \Psi\left(\varepsilon_{kl}, E_l\right) = \frac{1}{2} C_{ijkl} \varepsilon_{kl} \varepsilon_{ij} - e_{lij} E_l \varepsilon_{ij} - \frac{1}{2} \kappa_{il} E_l E_i - C_{ijkl} \varepsilon_{kl}^{\mathrm{irr}} \varepsilon_{ij} + \\ + e_{ikl} \varepsilon_{kl}^{\mathrm{irr}} E_i - P_i^{\mathrm{irr}} E_i, \end{aligned} \tag{5}$$

where the strain ε_{kl} and the electric field E_l are chosen as independent variables, C_{ijkl}, e_{lij} and κ_{il} are the elastic, piezoelectric and dielectric tensors. The partial derivatives of Ψ with respect to ε_{ij} and E_i lead to the constitutive equations:

$$\sigma_{ij} = \left.\frac{\partial \Psi}{\partial \varepsilon_{ij}}\right|_E = C_{ijkl}\, \left(\varepsilon_{kl} - \varepsilon_{kl}^{\mathrm{irr}}\right) - e_{nij}\, E_n, \tag{6}$$

$$D_i = -\left.\frac{\partial \Psi}{\partial E_i}\right|_\varepsilon = e_{ikl}\, \left(\varepsilon_{kl} - \varepsilon_{kl}^{\mathrm{irr}}\right) + \kappa_{in}\, E_n + P_i^{\mathrm{irr}}. \tag{7}$$

The domain structure of tetragonal ferroelectrics exhibits $90°$ and $180°$ domain walls (see Fig. 2). Following a model introduced by HUBER et al. [2], each possible polarization direction

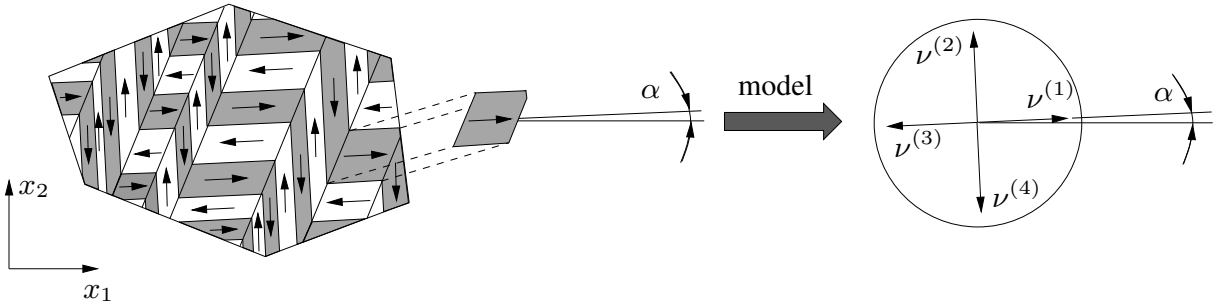

Figure 2. Domain structure of a single grain and motivation of the internal variable $\nu^{(n)}$

in a grain is weighted by an internal variable $\nu^{(n)}$ where $n = 1, \ldots, 4$ for a two-dimensional case. Here, the domain structure of a grain is represented by an arrowed cross at a single local material point. An evolution law for the internal variables $\nu^{(n)}$ is sought. HWANG et al. [1] formulated a local switching criterion, where the dissipative work $w^{\mathrm{diss}(n)}$ associated with the switching of a domain species n is related to a threshold value $w^{\mathrm{crit}} > 0$. Switching of a domain species occurs, if

$$w_{(\beta)}^{\mathrm{diss}(n)} \geq w_{(\beta)}^{\mathrm{crit}} \quad , \quad n = 1, \ldots, 4. \tag{8}$$

The subscript in Eq. (8) distinguishes between $\pm 90^\circ$ and 180° domain variants. The left side of Eq. (8) is given by:

$$w_{(\beta)}^{\mathrm{diss}(n)} = \sigma_{ij}\, \varepsilon_{ij(\beta)}^{\mathrm{sp}(n)} + E_i\, P_{i(\beta)}^{\mathrm{sp}(n)}. \tag{9}$$

An extension of the dissipative work w^{diss} is recommended by KESSELER AND BALKE [5] accounting for higher order terms. These terms are small in comparison to the terms outlined in Eg. (9). Therefore, they are neglected. The evolution equation for each $\nu^{(n)}$ is described by:

$$\mathrm{d}\nu^{(n)} = -\mathrm{d}\nu_0\, \mathcal{H} \left(\frac{w^{\mathrm{diss}(n)}}{w_{(\beta)}^{\mathrm{crit}}} - 1 \right) \quad , \quad w^{\mathrm{diss}(n)} = \max \left\{ w_{(\beta)}^{\mathrm{diss}(n)} \right\}. \tag{10}$$

The quantity $\mathrm{d}\nu_0$ is a model parameter and the Heaviside function $\mathcal{H}$ is equal to zero in case of $w^{\mathrm{diss}(n)} < w_{(\beta)}^{\mathrm{crit}}$ or equal to one if $w^{\mathrm{diss}(n)} \geq w_{(\beta)}^{\mathrm{crit}}$. Threshold values for different switching variants of a tetragonal unit cell can be found by, e.g. in [3]. The evolution equation is thermodynamically consistent since Eq. (10) is based on Eq. (9), the latter satisfying the CLAUSIUS-DUHEM-inequality (4), if $q_i = 0$.

A variety of grains with different orientations shall be considered in a representative volume element (RVE). Following Fig. 1, all grains in an RVE are condensed to one global material point which exhibits all possible domain orientations of an RVE. However, switching can only occur within the four species of a grain. In a FE approach a grain can be interpreted as an integration point, intrinsically accounting for grain interaction. A grain interaction in the condensed model is realized by an averaging technique.

On the macroscopic scale, represented by the RVE, stress and electric displacement are microscopic volume averages (s. [6]):

$$\langle \sigma_{ij} \rangle = \frac{1}{V} \int\limits_V \sigma_{ij}\,(x_l)\ \mathrm{d}V \quad , \quad \langle D_i \rangle = \frac{1}{V} \int\limits_V D_i\,(x_l)\ \mathrm{d}V. \tag{11}$$

In the following, the averages are specified by squared brackets. Assuming homogeneous fields in a grain m the volume $V^{(m)}$ and an equal size for each grain, i.e. $\sigma_{ij}^{(m)}$, $D_i^{(m)} = \text{const}$ in $V^{(m)}$ and $V = M\,V^{(m)}$, the averages result in:

$$\langle \sigma_{ij} \rangle = \frac{1}{M} \sum_{m=1}^{M} \sigma_{ij}^{(m)} \quad , \quad \langle D_i \rangle = \frac{1}{M} \sum_{m=1}^{M} D_i^{(m)}. \tag{12}$$

The resulting material coefficients of an RVE $\langle C_{ijkl} \rangle$, $\langle e_{ikl} \rangle$ and $\langle \kappa_{ij} \rangle$ are determined likewise.

Next, Eqs. (6) and (7) are formulated for each grain m, relating the quantities $\sigma_{ij}^{(m)}$, $D_i^{(m)}$, $E_n^{(m)}$ and $\varepsilon_{kl}^{(m)}$. In the following a generalized Voigt approximation is assumed. Therefore, strain and electric field are homogeneous in the RVE and thus equal in each grain. Bearing in mind Eq. (12), the average stress $\langle \sigma_{ij} \rangle$ and electric displacement $\langle D_i \rangle$ result in:

$$\langle \sigma_{ij} \rangle = \langle C_{ijkl}\,\rangle \overline{\varepsilon}_{kl} - \langle C_{ijkl}\,\varepsilon_{kl}^{\mathrm{irr}} \rangle - \langle e_{nij} \rangle \overline{E}_n, \tag{13}$$

$$\langle D_i \rangle = \langle e_{ikl} \rangle\, \overline{\varepsilon}_{kl} - \langle e_{ikl}\,\varepsilon_{kl}^{\mathrm{irr}} \rangle + \langle \kappa_{in} \rangle\, \overline{E}_n + \langle P_i^{\mathrm{irr}} \rangle. \tag{14}$$

The bars on $\overline{\varepsilon}_{kl}$ and $\overline{E}_n$ indicate the variables which are kept constant in the homogenisation procedure. Depending on the specific boundary value problem, the unknown quantities are chosen among the macroscopic stress $\langle \sigma_{ij} \rangle$, electric displacement $\langle D_i \rangle$, strain $\overline{\varepsilon}_{kl}$ and electric field $\overline{E}_n$. In the following, $\langle \sigma_{ij} \rangle = \sigma_{ij}^{\mathrm{ext}}$ and $\overline{E}_n = E_n^{\mathrm{ext}}$ are prescribed as boundary conditions. The strain $\overline{\varepsilon}_{kl}$ results from Eq. (13):

$$\overline{\varepsilon}_{kl} = \langle C_{ijkl} \rangle^{-1} \left\{ \sigma_{ij}^{\mathrm{ext}} + \langle C_{ijno}\,\varepsilon_{no}^{\mathrm{irr}} \rangle + \langle e_{rij} \rangle E_r^{\mathrm{ext}} \right\}. \tag{15}$$

The residual stress of a grain m resulting form domain wall motion, is then given by:

$$\sigma_{ij}^{(m)} = C_{ijkl}^{(m)} \left(\langle C_{ijkl} \rangle^{-1} \left\{ \sigma_{pq}^{\mathrm{ext}} + \langle C_{pqno}\,\varepsilon_{no}^{\mathrm{irr}} \rangle + \langle e_{rpq} \rangle E_r^{\mathrm{ext}} \right\} - \varepsilon_{kl}^{\mathrm{irr}(m)} \right) - e_{lij}^{(m)} E_r^{\mathrm{ext}}. \tag{16}$$

Other boundary conditions can be chosen, e.g. $\sigma_{ij}^{\mathrm{ext}}$ and D_i^{ext}, however they are not investigated here.

3. MODELING DAMAGE EVOLUTION IN FERROELECTRICS

A continuum damage approach for brittle ferroelectrics is presented in the following. The defect phase consists of cracks, randomly and dilutely distributed in the material, i.e. neglecting crack interactions. The constitutive damage model is implemented within the context of the condensed approach introduced in section 2.

3.1 Effective material properties in ferroelectrics

To calculate effective material properties, a linear material behavior of the cracked ferroelectric solid is considered in each load increment. Two out of four possible formulations of the constitutive behavior are (e.g. [7], [3]):

$$\begin{pmatrix}\varepsilon_{ij}\\ E_i\end{pmatrix} = \begin{pmatrix}S^*_{ijkl} & d^*_{lij}\\ -d^*_{ikl} & \beta^*_{il}\end{pmatrix}\begin{pmatrix}\sigma_{kl}\\ D_l\end{pmatrix} \quad , \quad \begin{pmatrix}\sigma_{ij}\\ D_i\end{pmatrix} = \begin{pmatrix}C^*_{ijkl} & -e^*_{lij}\\ e^*_{ikl} & \kappa^*_{il}\end{pmatrix}\begin{pmatrix}\varepsilon_{kl}\\ E_l\end{pmatrix}. \tag{17}$$

Here, S_{ijkl}, d_{rij} and β_{ir} describe the elastic compliance, piezoelectric constants and dielectric impermeability, respectively and $*$ denotes effective properties. C_{ijkl}, e_{ikl} and κ_{il} are the previously introduced stiffness, piezoelectric and dielectric constants. In a compressed notation Eq. (17) can be written as:

$$Z_p = F^*_{pq}\,\Pi_q \quad , \quad \Pi_p = C^*_{pq}\,Z_q. \tag{18}$$

The variables in Eq. (18) describe generalized values for strain Z_p, stress Π_q, stiffness C_{pq} and compliance F_{pq}, where indices p, q run from 1 to 9. Following e.g. [6], [8] and [9], Z_p can be decomposed into a matrix part Z^{M}_p and a part Z^{C}_p representing the defect phase:

$$Z_p = Z^{\mathrm{M}}_p + Z^{\mathrm{C}}_p. \tag{19}$$

Based on this assumption, Eq. (18) can be written for the matrix phase as:

$$Z^{\mathrm{M}}_p = F^{\mathrm{M}}_{pq}\,\Pi^{\mathrm{M}}_q \quad , \quad \Pi^{\mathrm{M}}_p = C^{\mathrm{M}}_{pq}\,Z^{\mathrm{M}}_q. \tag{20}$$

Inserting Eq. (19) into Eq. (20) leads to relationships between the matrix and the cracked phase:

$$Z_p = F^{\mathrm{M}}_{pq}\,\Pi_q + Z^{\mathrm{C}}_p \quad , \quad \Pi^{\mathrm{M}}_p = C^{\mathrm{M}}_{pq}\left(Z_q - Z^{\mathrm{C}}_q\right). \tag{21}$$

Two different cases will be discussed in the following: a generalized REUSS assumption, where generalized stresses are constant and therefore $Z^{\mathrm{C}}_p = F^{\mathrm{C}}_{pq}\,\Pi^{\infty}_q$ and a generalized VOIGT approximation, where generalized strains are constant leading to $Z^{\mathrm{C}}_p = D_{pq}\,Z^{\infty}_q$. F^{C}_{pq} and D_{pq} are the influence tensors and Π^{∞}_q and Z^{∞}_q describe the loading conditions of the RVE. The effective material coefficients of the REUSS approximation result from Eqs. (18), (21) and the corresponding definition of the cracked phase Z^{C}_p:

$$\begin{aligned} F^*_{pq} &= F^{\mathrm{M}}_{pq} + F^{\mathrm{C}}_{pq},\\ C^*_{pq} &= \left(F^{\mathrm{M}}_{pq} + F^{\mathrm{C}}_{pq}\right)^{-1}. \end{aligned} \tag{22}$$

For the VOIGT assumption, the effective coefficients follow from applying Eqs. (18), (21) and Z^{C}_p of the VOIGT approximation:

$$\begin{aligned} C^*_{pq} &= C^{\mathrm{M}}_{pr}\,\left(\delta_{rq} - D_{rq}\right),\\ F^*_{pq} &= \left\{C^{\mathrm{M}}_{pr}\,\left(\delta_{rq} - D_{rq}\right)\right\}^{-1}. \end{aligned} \tag{23}$$

Deriving the relations (22) and (23), it has to be borne in mind that $F_{pq}^{-1} = C_{pq}$. Further, $\Pi_p = \Pi_p^M$ is assumed. Mechanically, this implies a stress-free defect phase which holds in the case of voids or cracks. From the electrostatic point of view, impermeable crack boundary conditions are modeled.

3.2 Modeling of the defect phase

For the calculation of the effective material constants at a local material point m, the crack RVE with an edge length of $\sqrt{A}$ shown in Fig. 3 is considered. There are several cracks with

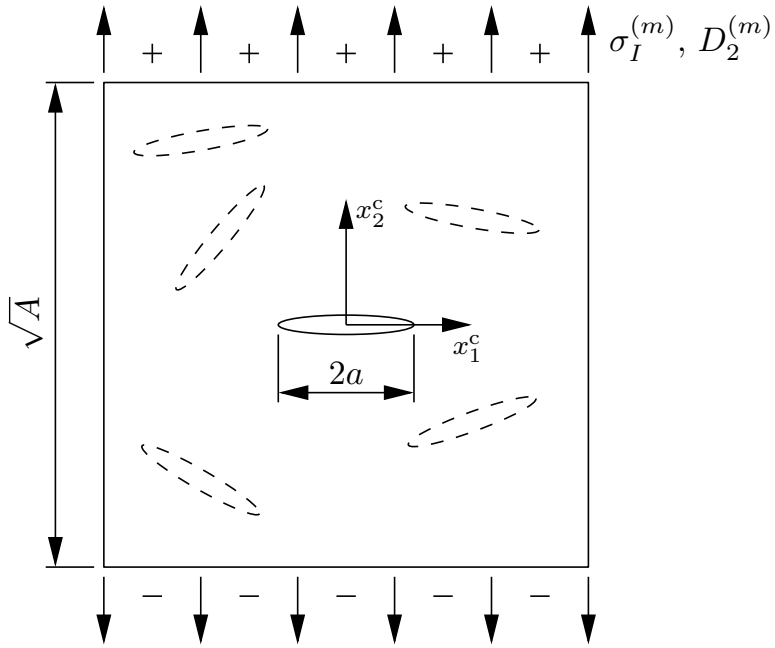

Figure 3. Model of the defect phase in an RVE m under electromechanical loading

different orientations under an electromechanical loading $\sigma_I^{(m)}$ and $D_2^{(m)}$. Due to the dilute or noninteracting assumption [10], the model of the defect phase can be reduced to one single crack in an unbounded medium, where the edge length of the crack RVE is just a parameter to introduce the crack density. The coordinate system of the crack is defined by x_1^{c} and x_2^{c}. Further, only cracks perpendicular to the principle stress $\sigma_I^{(m)}$ are considered, since these are the most critical ones. Thus, the local crack coordinate system and the orientation of the defect RVE coincide with the principal axes of the stress field. Electric loads parallel to the crack faces $D_1^{(m)}$ are not considered, since they are dispensable from the fracture mechanical point of view, at least concerning classical theories. Advanced models of piezoelectric fracture mechanics, however, reveal effects going along with electric fields parallel to the crack faces [11]. Even collinear stress loads $\bar{\sigma}_{11}$ may have an impact on the mode I SIF [12]. The principal stresses

$\sigma_{I,II}^{(m)}$ of a local material point m are calculated as follows:

$$\sigma_{I,II}^{(m)} = \frac{1}{2}\left(\sigma_{11}^{(m)} + \sigma_{22}^{(m)}\right) \pm \sqrt{\frac{1}{4}\left(\sigma_{11}^{(m)} + \sigma_{22}^{(m)}\right)^2 + \left(\sigma_{12}^{(m)}\right)^2}, \tag{24}$$

with $\sigma_{I}^{(m)} > \sigma_{II}^{(m)}$. Following Fig. 3, the crack density

$$f = \frac{4a^2}{A} \tag{25}$$

is introduced as a relationship of the squares of the crack length $2a$ and the edge length $\sqrt{A}$.

Boundary conditions on the crack surfaces and relevant coordinate systems are illustrated in Fig 4. Here, an impermeable crack is considered, following the Neumann type boundary

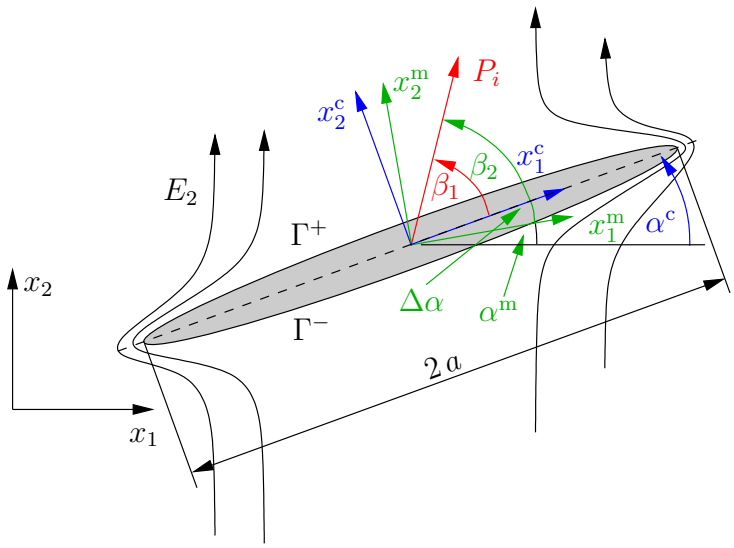

Figure 4. Coordinate systems and parameters of an arbitrarily orientated impermeable crack

condition investigated e.g. by [13] and [14]. Therefore, the crack faces are free of charges, i.e.

$$D_2^+\left(x_1^{\mathrm{c}}\right) = D_2^-\left(x_1^{\mathrm{c}}\right) = 0 \tag{26}$$

on the positive Γ^+ and negative Γ^- crack surfaces.

Besides the global coordinate system $(x_1,\, x_2)$, other coordinate systems are relevant for the development of the damage model. The one related to the local material point m, following the idea of the condensed approach depicted in Fig. 1, is denoted by $(x_1^{\mathrm{m}},\, x_2^{\mathrm{m}})$, β_1 and β_2 describe the orientation of the polarisation direction with respect to x_1^{c} and x_1^{m}. α^{c} and α^{m} denote the orientations of the local coordinate systems of the crack and the material RVE related to $(x_1^m,\, x_2^m)$. The angle between these two systems is defined as $\Delta\alpha = \alpha^{\mathrm{c}} - \alpha^{\mathrm{m}}$. The different angles, shown in Fig. 4, are relevant for the calculation of the Irwin matrix (see e.g. [15]) and the effective material constants.

The jump of generalized displacements Δu_M at the crack faces in a ferroelectric ceramic under an electromechanical loading was discussed e.g. by [16], [15] and [12]. With the impermeable boundary condition introduced in Eq. (26) and bearing in mind that a two-dimensional case is supposed, Δu_M is given by:

$$\begin{aligned}\Delta u_M = \begin{pmatrix}\Delta u_1\\ \Delta u_2\\ \Delta\varphi\end{pmatrix} &= 2\begin{pmatrix}Y_{11} & Y_{12} & Y_{14}\\ Y_{21} & Y_{22} & Y_{24}\\ Y_{41} & Y_{42} & Y_{44}\end{pmatrix}\begin{pmatrix}0\\ \sigma_I\\ D_2^\infty\end{pmatrix}\sqrt{a^2-\left(x_1^{\mathrm{c}}\right)^2},\\ &= 2\,Y_{MN}\,\Sigma_N\sqrt{a^2-\left(x_1^{\mathrm{c}}\right)^2},\end{aligned} \tag{27}$$

where Y_{MN} is the Irwin matrix depending on material constants and the orientation of the crack with respect to the poling direction. To calculate the effective material properties of a microscopic RVE, following the REUSS or VOIGT approximations, the strain and electric field of the defect phase are given by:

$$\langle\varepsilon_{ij}\rangle^{\mathrm{C}} = \frac{1}{2A}\int_{-a}^{a}\left(\Delta u_i n_j + \Delta u_j n_i\right)\,\mathrm{d}x_1^{\mathrm{c}} \quad , \quad \langle E_i\rangle^{C} = -\frac{1}{A}\int_{-a}^{a}\Delta\varphi\, n_i\,\mathrm{d}x_1^{\mathrm{c}}, \tag{28}$$

where n_i is the unit normal on the positive crack face and the part for the strain is classical (see e.g. [6]). The influence tensor F_{pq}^{C} according to Eq. (22) is hence determined as

$$F_{pq}^{\mathrm{C}} = \frac{1}{4}\pi\, f\begin{pmatrix}0 & 0 & 0 & 0 & 0\\ 0 & Y_{22} & 0 & 0 & Y_{24}\\ 0 & Y_{12} & 0 & 0 & Y_{14}\\ 0 & 0 & 0 & 0 & 0\\ 0 & -Y_{42} & 0 & 0 & -Y_{44}\end{pmatrix}. \tag{29}$$

Assuming a generalized VOIGT approximation, the influence tensor D_{pq} results from the REUSS approximation by replacing Π_q^∞ by Z_q^∞ via the constitutive equations (17):

$$D_{km} = \frac{1}{4}\pi\, f\begin{pmatrix}0 & 0 & 0\\ Y_{22}C_{21}^{\mathrm{M}} + Y_{24}e_{21}^{\mathrm{M}} & Y_{22}C_{22}^{\mathrm{M}} + Y_{24}e_{22}^{\mathrm{M}} & Y_{22}C_{23}^{\mathrm{M}} + Y_{24}e_{23}^{\mathrm{M}}\\ Y_{12}C_{21}^{\mathrm{M}} + Y_{14}e_{21}^{\mathrm{M}} & Y_{12}C_{22}^{\mathrm{M}} + Y_{14}e_{22}^{\mathrm{M}} & Y_{12}C_{23}^{\mathrm{M}} + Y_{14}e_{23}^{\mathrm{M}}\\ 0 & 0 & 0\\ -Y_{42}C_{21}^{\mathrm{M}} - Y_{44}e_{21}^{\mathrm{M}} & -Y_{42}C_{22}^{\mathrm{M}} - Y_{44}e_{22}^{\mathrm{M}} & -Y_{42}C_{23}^{\mathrm{M}} - Y_{44}e_{23}^{\mathrm{M}}\end{pmatrix}\begin{pmatrix}0 & 0\\ Y_{24}\kappa_{21}^{\mathrm{M}} - Y_{22}e_{12}^{\mathrm{M}} & Y_{24}\kappa_{22}^{\mathrm{M}} - Y_{22}e_{22}^{\mathrm{M}}\\ Y_{14}\kappa_{21}^{\mathrm{M}} - Y_{12}e_{12}^{\mathrm{M}} & Y_{14}\kappa_{22}^{\mathrm{M}} - Y_{12}e_{22}^{\mathrm{M}}\\ 0 & 0\\ Y_{42}e_{12}^{\mathrm{M}} - Y_{44}\kappa_{21}^{\mathrm{M}} & Y_{42}e_{22}^{\mathrm{M}} - Y_{44}\kappa_{22}^{\mathrm{M}}\end{pmatrix}. \tag{30}$$

Finally, it should be mentioned that the local polarisation directions $\beta_{1/2}$, see Fig. 4, depend on the microstructural evolution due to domain switching, see Sec. 2, thus being subject to a permanent change during the loading process. Therefore, the effective material properties and the Irwin matrix have to be recalculated after each switching increment $\mathrm{d}\nu$.

3.3 An accumulation model for high cycle fatigue and lifetime prediction

The condensed approach outlined in Sec. 2 is exploited in regard to high cycle fatigue. The damage evolution is based on subcritical crack growth governed by the classical Paris law [17]. Most investigations about fatigue damage of ferroelectrics under electromechanical loading deal with low cycle fatigue from an experimental or modeling point of view (e.g. [18], [19] and [20]). For high cycle fatigue, a cycle by cycle simulation is unrealistic due to the high effort and computational costs. The idea presented in the following is based on an accumulation of many physical cycles N_P and their mapping onto much less numerical ones N.

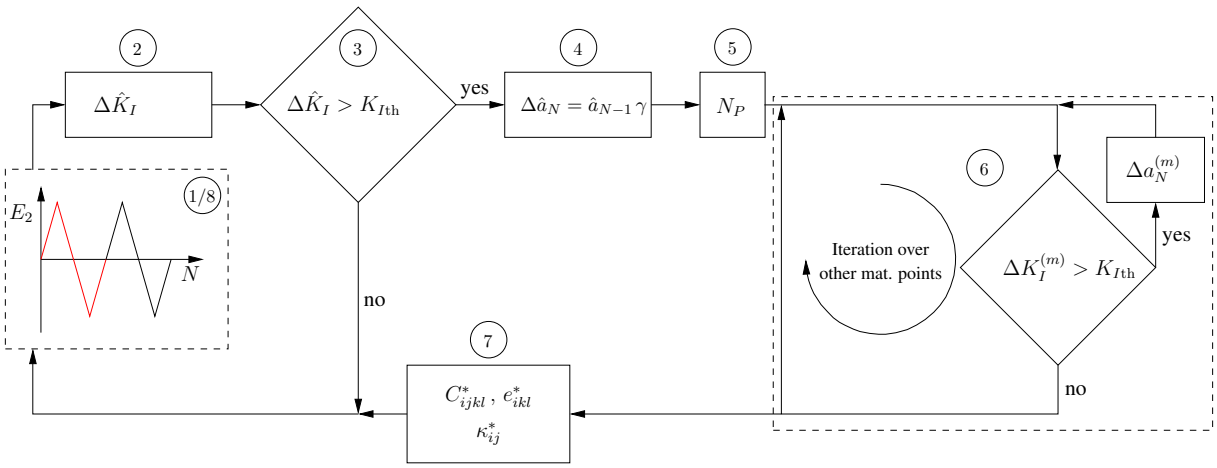

Figure 5. Calculation scheme for high cycle fatigue damage prediction based on the condensed model

The calculation scheme is captured in Fig. 5 and includes eight steps. In the first step, one load cycle N is simulated applying the approach outlined in section 2. Next, the material RVE with the maximum peak-to-peak stress intensity factor (SIF) $\Delta\hat{K}_I$ is sought. The SIF at a local material point m is calculated as

$$\Delta K_I^{(m)} = \Delta\sigma_I^{(m)}\sqrt{\pi\, a_0} \tag{31}$$

with $\Delta\sigma_I^{(m)} = \sigma_I^{\max(m)} - \sigma_I^{\min(m)}$. σ_I results from Eq. (24) and ΔK_I will be simply denoted as SIF in the following. In the third step it is checked if $\Delta\hat{K}_I$ is larger than or equal to the threshold value $K_{I\mathrm{th}}$. If this criterion is not satisfied, the next load cycle is simulated. Otherwise, the crack propagation increment $\Delta\hat{a}_N$ is determined as follows:

$$\Delta\hat{a}_N = \gamma\,\hat{a}_{N-1}. \tag{32}$$

Notice, that the initial crack length is a_0. Again, the superscript hat refers to the material point with the maximum principal stress. γ is a numerical parameter describing the ratio of the increment Δa and the crack length. Therefore, the new crack length $\hat{a}_N$ is obtained as:

$$\hat{a}_N = (1+\gamma)\ \hat{a}_{N-1}. \tag{33}$$

While the aforementioned load cycles N have a pure numerical background, the number of physical cycles N_P associated with the crack growth increment $\Delta\hat{a}_N$, is the relevant quantity. Thus, in the next step, N_P is determined from the classical Paris law [17]

$$\frac{\mathrm{d}a}{\mathrm{d}N} = C\left(\Delta K_I\right)^{\eta}\ . \tag{34}$$

C and η are material-dependent parameters. Separation of crack length and number of cycles under consideration of Eq. (31) leads to

$$\int_0^{N_P} \mathrm{d}N = \int_{a_{N-1}}^{a_N} \frac{\mathrm{d}a}{C\left(\Delta\sigma_I\sqrt{\pi a}\right)^{\eta}}\ . \tag{35}$$

Integration of both sides of Eq. (35) and assuming that the peak-to-peak value $\Delta\sigma_I$ is constant during one numerical cycle N yields

$$N_P = \frac{2}{C\left(2-\eta\right)\left(\Delta\sigma_I\sqrt{\pi}\right)^{\eta}}\left[\left(\hat{a}_{N-1}\left(1+\gamma\right)\right)^{\frac{2-\eta}{2}} - \hat{a}_{N-1}^{\frac{2-\eta}{2}}\right]\ . \tag{36}$$

In step six of Fig. 5 the crack propagation $\Delta a_N^{(m)}$ in each of the other local material points m is determined from Eq. (34) as a function of N_P, $\Delta\sigma_I^{(m)}$ and $a_{N-1}^{(m)}$:

$$\Delta a_N^{(m)} = C\left(\Delta\sigma_I^{(m)}\sqrt{\pi a_{N-1}^{(m)}}\right)^{\eta} N_P. \tag{37}$$

A simplifying assumption of Eq. (37) is that the crack length is constant for the integration. After having calculated all $\Delta a_N^{(m)}$, the effective material constants are determined according to the introduced averaging technique in Sec. 2. Now, the next numerical load cycle is simulated based on the updated crack lengths.

The scheme is repeated assembling the physical cycles to obtain their total number, finally representing the life time of the structure under electromechanical loading. The simulation is stopped, as soon as a rupture criterion is satisfied. Here, the average damage variable or crack density parameter $\langle f\rangle$, respectively, reaches a critical value, e.g. 0.5. Following the weakest link interpretation, the simulation can also be controlled by the material point $\hat{m}$, which in the first load cycle has been identified as the one with the highest stress level. Then, just the crack density $\hat{f}^{(m)}$ is inserted into the rupture criterion. The progress of damage in the other material points, however, still has an impact on the predicted life time by influencing the evolution of effective elastic, piezoelectric and dielectric constants. These material properties are in turn decisive for the domain induced residual stresses which are significantly controlling the damage process.

4. RESULTS OF LIFETIME PREDICTION

All calculations are based on the material data of barium titanate taken from [21]. The constants for the Paris law have been taken from [22], where experiments on fatigue crack growth in PZT under pure mechanical loading are presented. The values of C and η have been adopted here, since there are not any other experimental data in this field.

First, the influence of a bipolar and an unipolar electrical loading is investigated. Mechanically, the specimen is neither clamped nor submitted to a traction load. The loading scheme is shown in Fig. 6 (a) in terms of the normalized electric field vs. the first numerical load cycles. In Fig. 6 (b) the crack density f normalized with respect to the initial damage f_0 is plotted vs. the accumulated number of physical cycles. It becomes obvious, that the damage evolution

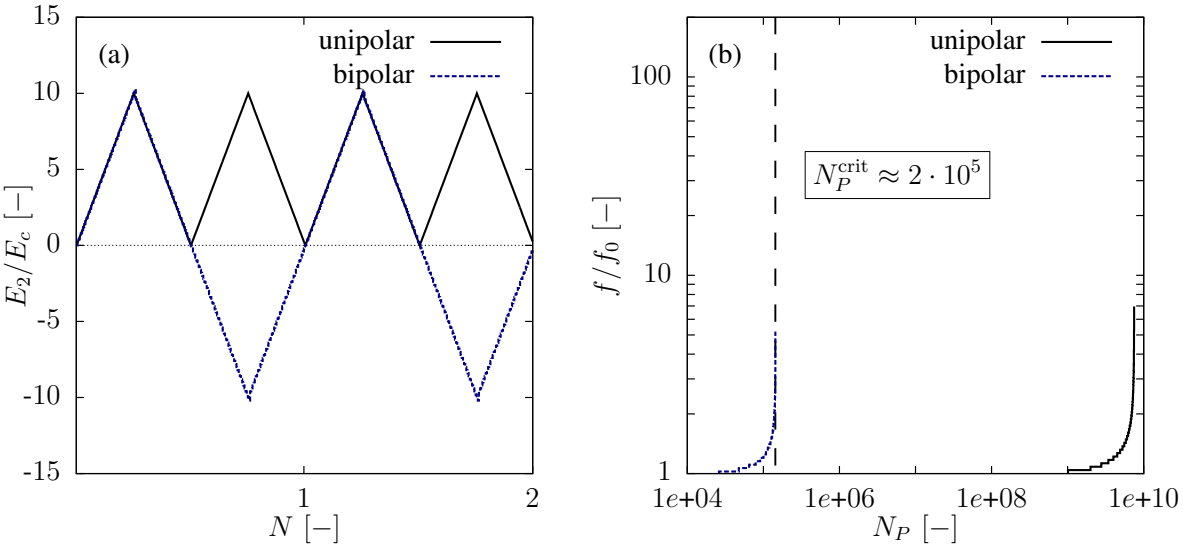

Figure 6. Comparison of bipolar and unipolar electric loading: loading schemes (a) and damage evolution (b)

exhibits an asymptotic behavior. The critical lifetime results with a sufficient accuracy from the vertical tangent. Therefore, in Fig. 6 (b) a lifetime of $N_P^{\text{crit}} \approx 2 \cdot 10^5$ is given for the bipolar loading scheme and $N_P^{\text{crit}} \approx 7 \cdot 10^9$ for the unipolar loading scheme. The results presented in the following are based on unipolar loading. The solid line is thus denoted as reference simulation in the following.

In Fig. 7 (a) the influence of the initial crack density f_0 on the critical number of cycles is shown. It is obvious, that an increasing initial crack density results in a decreasing number of cycles and therefore a decreasing lifetime. Fig. 7 (b) presents the influence of the parameters of the PARIS law, following Eq. (34). Fundamental finding of Fig. 7 (b) is a crucial influence of the parameters C and η on the number of critical cycles. Especially η is a very sensitive parameter. Bearing in mind, that C and η are taken from PZT and not be known for $\mathrm{BaTiO_3}$, the results of the predictions presented in this paper have to considered as qualitative.

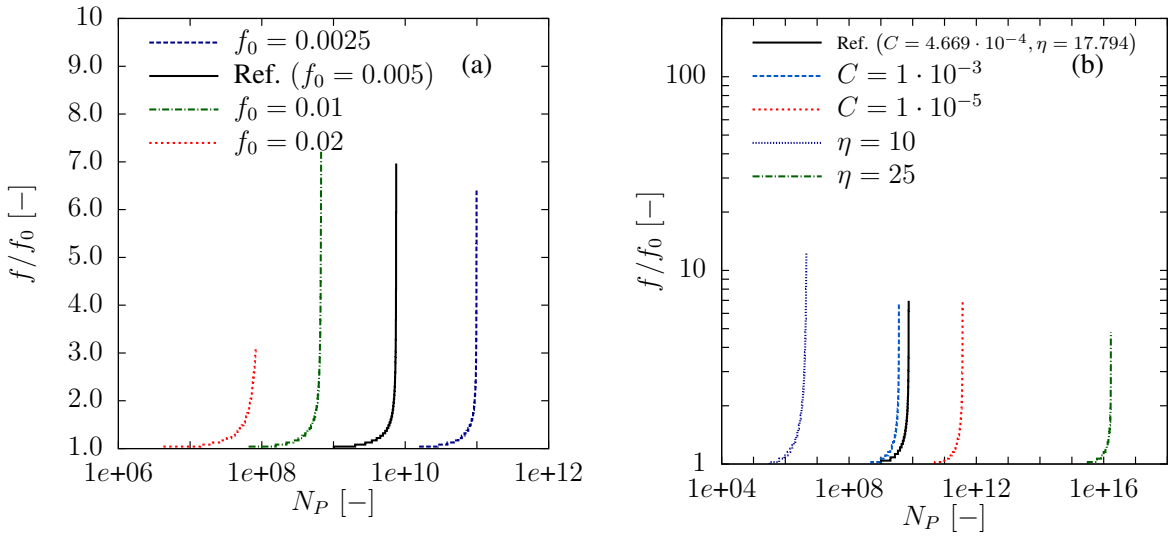

Figure 7. Influence of the initial crack density (a) and the parameters of the PARIS law (b) on the lifetime

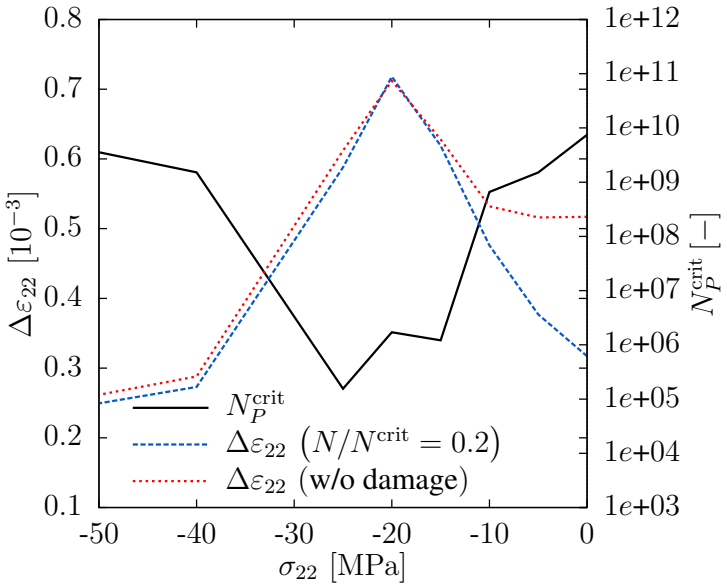

Figure 8. Influence of a compressive preload on actuation strain and life time. The dotted line represents the strain in an undamaged structure

In Fig. 8 the influence of an electromechanical loading on the lifetime and the actuation strain is investigated. The initial crack density f_0 and the parameters C and η are the same as for the solid lines in Fig. 7. The amplitude of the unipolar loading scheme is $10\,E_c$. Current experimental investigations show on the one hand that a mechanical compressive preloading into the direction of the electric field fosters the poling and thus the actuation strain within a certain

stress range [23, 24, 25]. On the other hand, a reduction of the lifetime due to compressive preloading has recently been observed [26]. Both effects are shown in Fig. 8. The solid line represents the number of critical cycles, the dashed line the actuation strain and the dotted line represents the actuation strain in an undamaged structure. Main findings of Fig. 8 are as follows: Increasing compressive preloading reduces the influence of damage on the actuation efficiency $\Delta\varepsilon_{22}$ and at a compressive preload of $\sigma_{22} = -15\,\mathrm{MPa}$, the difference between an undamaged and damaged structure becomes negligible. The actuation efficiency becomes a maximum at $\sigma_{22} = -20\,\mathrm{MPa}$ and goes along with a lifetime reduction of 40 percent in comparison to the stress-free loading condition. An increasing compressive preloading below $\sigma_{22} = -20\,\mathrm{MPa}$ finally results in a decreasing actuation efficiency and a recovering of the lifetime.

5. CONCLUSIONS

A condensed approach for tetragonal ferroelectrics has been presented based on a homogenisation technique and the effective medium theory. Being mechanically and electrostatically consistent and evolved from a thermodynamical framework, it provides a powerful and efficient tool to investigate the inelastic constitutive behavior of multifunctional materials. In contrast to FE approaches, a spacial discretisation is not necessary and both implementation and computation efforts are comparably low. Concerning damage predictions in ferroelectrics, it is essential that residual stresses are accurately obtained from a modeling approach, since they provide the major contribution to the loading of microcracks or other defects. The constitutive framework describes an evolution of the microstructure in terms of domain wall motion and the growth of microcracks. Due to the influence of the state of damage on the effective elastic, dielectric and piezoelectric properties, there is a mutual interaction between both irreversible mechanisms. Results are discussed in terms of life time predictions under high cycle electric loading conditions, requiring an approach to efficiently handle up to 10^{10} load cycles. To improve the predictions quantitatively, more sophisticated models have to be established accounting e.g. for crack interactions or nontrivial boundary conditions at crack faces. Also, the influence of an electric field is just taken into account on the loading side by controlling the residual stress. This might be the major contribution, however it has to be borne in mind that the intrinsic material resistance may also depends on electric fields. Finally, to get closer to applied research, the constitutive behavior of modern ferroelectric materials, including morphotropic or lead-free compositions, has to be a subject of advanced modeling.

References

[1] S. C. Hwang, C. S. Lynch, and R. M. McMeeking. Ferroelectric/ferroelastic interactions and a polarization switching model. *Acta metall. mater.*, 43:2073–2084, 1995.

[2] J. E. Huber, N. A. Fleck, C. M. Landis, and R. M. McMeeking. A constitutive model for ferroelectric polycrystals. *J mech. phys. solids*, 47:1663–1697, 1999.

[3] S. Lange and A. Ricoeur. A condensed microelectromechanical approach for modeling tetragonal ferroelectrics. *Int. J. Solids Struct.*, 54:100–110, 2015.

[4] V. Z. Parton and B. A. Kudryavtsev. *Electromagnetoelasticity*. Gordon and Breach Science Publishers, New York, 1988.

[5] Hannes Kessler and Herbert Balke. On the local and average energy release in polarization switching phenomena. *J. Mech. Phys. Solids*, 49:953–978, 2001.

[6] Dietmar Gross and Thomas Seelig. *Fracture Mechanics: With an introduction to Micromechanics*. Springer Verlag, Berlin, 2011.

[7] R. Gellmann and A. Ricoeur. Extended semi-analytical investigations of crack growth resistamce behavior in ferroelectric materials. *Acta Mech.*, 223:2357–2368, 2012.

[8] X.D. Wang and L.Y. Jiang. The effective electroelastic property of piezoelectric media with parallel dielectric cracks. *Int. J. Solids Struct.*, 40:5287–5303, 2003.

[9] Romann Gellmann, Andreas Ricoeur, Eugen Merkel, and Zhibin Wang. Generalized boundary conditions and effective properties in cracked piezoelectric solids. *Proc. Appl. Math. Mech.*, 13:225–226, 2013.

[10] Mark Kachanov. Effective elastic properties of cracked solids: critical review of some basic concepts. *Appl. Mech. Rev.*, 45:304–335, 1992.

[11] Andreas Ricoeur, Roman Gellmann, and Zhibin Wang. Influence of inclined electric fields on the effective fracture toughness of piezoelectric ceramics. *Acta Mech.*, 226:491–503, 2014.

[12] Roman Gellmann and Andreas Ricoeur. Some new aspects of boundary conditions at cracks in piezoelectrics. *Arch. Appl. Mech.*, 82:841–852, 2012.

[13] H. Sosa. On the fracture mechanics of piezoelectric solids. *Int. J. Solids Struct.*, 29:1–15, 1990.

[14] Z. Suo. Models for breakdown-resistant dielectric and ferroelectric ceramics. *J. Mech. Phys. Solids*, 41:1155–1176, 1993.

[15] Andreas Ricoeur and Meinhard Kuna. Influence of electric fields on the fracture of ferroelectric ceramics. *J. Eur. Ceram. Soc.*, 23:1313–1328, 2003.

[16] Y.E. Pak. Linear electro-elastic fracture mechanics of piezoelectric materials. *Int. J. Fract.*, 54:79–100, 1992.

[17] P. Paris and F. Erdogan. A critical analysis of crack propagation laws. *J Basic Eng.*, 85:528–534, 1963.

[18] Ting Zhu and Wei Yang. Fatigue crack growth in ferroelectrics driven by cyclic electric loading. *J. Mech. Phys. Solids*, 47:81–97, 1999.

[19] Ilona Westram, William S. Oates, Doru C. Lupascu, Juergen Roedel, and Christopher Lynch. Mechanism of electric fatigue crack growth in lead zirconate titanate. *Acta Mater.*, 55:301–312, 2007.

[20] Ilona Westram, Andreas Ricoeur, Andreas Emmerich, Juergen Roedel, and Meinhard Kuna. Fatigue crack growth law for ferroelectrics under cyclic electrical and combined electromechanical loading. *J. Eur. Ceram. Soc.*, 27:2485–2494, 2007.

[21] B. Jaffe, W. R. Cook, and H. Jaffe. *Piezoelectric ceramics*. Academic Press, London, 1971.

[22] Christopher R. J. Salz, Mark Hoffman, Ilona Westram, and Jürgen Rödel. Cyclic fatigue crack growth in PZT under mechanical loading. *J Am. Ceram. Soc.*, 88:1331–1333, 2005.

[23] Robert Dittmer, Kyle G. Webber, Emil Aulbach, Wook Jo, Xiaoli Tan, and Jürgen Rödel. Electric-field-induced polarization and strain in $0.94(\mathrm{Ba_{1/2}Na_{1/2}})\mathrm{TiO_3} - 0.06\mathrm{BaTiO_3}$ under uniaxial stress. *Acta Mater.*, 61:1350–1358, 2013.

[24] Robert Dittmer, Kyle G. Webber, Emil Aulbach, Wook Jo, Xiaoli Tan, and Jürgen Rödel. Optimal working regime of lead-zirconate-titanate for actuation applications. *Sensor Actuat. A-Phys.*, 189:187–194, 2013.

[25] Dayu Zhou and Marc Kamlah. Dielectric and piezoelectric performance of soft PZT piezoceramics under simultaneous alternating electromechanical loading. *J. Eur. Ceram. Soc.*, 25:2415–2420, 2005.

[26] Faxin Li. Ultrahigh superelastic and actuation strains in ferroelectric crys- tals by reversible electromechanical domain switching. *In: 5th International Congress on Ceramics*, page 250, 2014.